Energy & Buildings 231 (2021) 110575

Contents lists available at ScienceDirect

Energy & Buildings

journal homepage: www.elsevier.com/locate/enb

Thermoregulation model JOS-3 with new open source code

Yoshito Takahashi [a,*], Akihisa Nomoto [a], Shu Yoda [a], Ryo Hisayama [a], Masayuki Ogata [b], Yoshiichi Ozeki [c], Shin-ichi Tanabe [a]

[a] Waseda University, Bldg. 55N-701, 3-4-1, Okubo, Shinjuku-ku, Tokyo 169-8555, Japan
[b] Tokyo Metropolitan University, Bldg. 9 734, 1-1, Minami-Osawa, Hachioji-shi, Tokyo 192-0397, Japan
[c] AGC Incorporated, 1-1, Suehiro-cho, Tsurumi-ku, Yokohama-shi, Kanagawa 230-0045, Japan

ARTICLE INFO

Article history:
Received 21 January 2020
Revised 24 September 2020
Accepted 17 October 2020
Available online 21 October 2020

Keywords:
Thermoregulation model
Open source code
Thermal comfort
Thermal response
Physiological response
Brown adipose tissue
Non-shivering thermogenesis
Shortwave solar radiation
Signal decrement by aging
Metabolic rate

ABSTRACT

A thermoregulation model, joint system thermoregulation model (JOS-3), was developed based on JOS-2. JOS-3 consists of 83 nodes, and human physiological responses and body temperatures are calculated using the backward difference method. In JOS-3, brown adipose tissue activity, aging effects, and heat gain by shortwave solar radiation at the skin, are installed to predict human physiological responses, considering personal characteristics in transient and non-uniform thermal environments. In addition, methods to determine shivering thermogenesis, sweating distribution, and basal metabolic rate were modified from those used in JOS-2. We coded JOS-3 in Python-3 and published the JOS-3 package. This model was validated by comparing its results with those of human subject tests conducted under stable and transient conditions. It was confirmed that JOS-3 has a higher accuracy for heat production in young and older subjects and mean skin temperature in older subjects than JOS-2 under cold environmental conditions. Moreover, JOS-3 was simulated in nine transient conditions. Consequently, the root mean-squared error (RMSE) of the rectal and mean skin temperatures between the predicted and experimental values were 0.12–0.38 and 0.58–0.83 °C, respectively.

1. Introduction

Predicted mean vote (PMV) [1] and standard new effective temperature (SET*) [2] are widely used as thermal comfort and health risk assessment indexes in steady and uniform thermal environments, but these indexes are difficult to apply in unsteady and non-uniform thermal environments [3]. In recent years, personal heating and cooling systems (personal comfort system: PCS) have been studied to effectively improve individual thermal comfort. Estimating the physiological and psychological responses of local human bodies in a non-uniform environment of PCS is essential to the quantitative evaluation of the environment. With respect to thermal sensations, new studies have shown the thermal sensitivity maps of hands, feet, and the whole body [4,5]. Thermoregulation models have been used for thermal comfort evaluations in unsteady and non-uniform environments. These models simulate human physical heat exchanges by conduction and blood flow in body tissues, and by convection, evaporation, and radiation between a body and ambient environments. In addition, they simulate physiological responses such as sweating, vasodilation, vasoconstriction, and shivering according to their body temperature. Almost all models consist of several body segments, such as the head and trunk, and each segment has several layers, including core, muscle, fat, and skin.

Thermoregulation models can be classified into lumped or distributed parameter models. The underlying calculation method of a thermoregulation model is based on the research by Wissler [6]. Gagge's 2-node model [2,7] and Stolwijk's model [8] are famous as lumped parameter models. Gagge's 2-node model is based on Stolwijk and Hardy's model [9] and consists of the core and skin; it is used for computation of ET* and SET* and forms the basis for Jones's [10] and Kohri's [11,12] model. Stolwijk's model [8] consists of a sphere head and five cylinders of other body segments; it is the basis for many thermoregulation models, such as those of Gordon et al. [13], Fiala et al. [14], Huizenga et al. [15], and Streblow et al. [16]. The control system of Fiala's model [14] is based on human subject tests covering a range of environmental temperatures between 5 and 50 °C and metabolic rates between 0.8 and 10.0 met. Fiala's vasomotion model improved the accuracy of core temperature prediction, which was one of the problems in the Stolwijk model. The Berkeley model by Huizenga et al. [15] is characterized by the effects of clothing layers and contact on a body surface. In addition, the model considered counter-current blood

* Corresponding author.
E-mail address: ytakahashi@tanabe.arch.waseda.ac.jp (Y. Takahashi).

https://doi.org/10.1016/j.enbuild.2020.110575
0378-7788/

Symbols

AGbat: aging factor of brown adipose tissue's volume [–]
AGbatinc: aging factor of brown adipose tissue's incidence [–]
AGci: aging factor of cardiac index [–]
AGdilat: aging factor of vasodilation [–]
AGshiv: aging factor of shivering [–]
AGstric: aging factor of vasoconstriction [–]
AGsweat: aging factor of sweating [–]
B: heat exchange by blood flow [W]
BAT: volume of brown adipose tissue [SUV]
BF: blood flow rate [L/h]
BFB: basal blood flow rate [L/h]
BFB_{all}: basal blood flow rate in the whole body [L/h]
BFB_{ra}: ratio of basal blood flow rate to that of the standard body [–]
BFB_{st}: basal blood flow rate of the standard body [–]
BMI: body mass index [kg/m^2]
BSA: body surface area [m^2]
BSA_{all}: body surface area in whole body [m^2]
BSA_{ra}: ratio of body surface area to that of the standard body [–]
BSA_{st}: body surface area of the standard body [m^2]
C: heat exchange at skin by convection [W]
Cap: heat capacity [J/K]
Mshiv: heat production by shivering [W]
Mshivf: distribution coefficient of heat production by shivering [–]
Mwork: heat production by external work [W]
Mworkf: distribution coefficient of heat production by shivering [W]
NST: non-shivering signal [W]
NSTmax: max non–shivering thermogenesis signal [W]
O_{ava}: opening rate of arteriovenous anastomoses (AVA) in Hand and Foot [–]
PAR: physical activity ratio [–]
Q: heat production [W]
R: heat exchange at skin by radiation [W]
SHIV: shivering signal [W]
SKINC: distribution coefficient of vasoconstriction [–]
SKIND: distribution coefficient of vasodilation [–]
SKINR: distribution coefficient of thermal receptor [–]
SKINS: distribution coefficient of sweating [–]
STRIC: vasoconstriction signal [–]
SW_{sk}: heat gain due to shortwave solar radiation at the skin [W]
SW_{dw}: downward horizontal shortwave radiation [W/m^2]
SW_{up}: upward horizontal shortwave radiation [W/m^2]
C_{st}: heat capacity of the standard body [J/K]
Cdt: heat conductance [W/K]
Cdt_{st}: heat conductance of the standard body [W/K]
CI: cardiac index [L/min/m^2]
Cld: error signal of cold receptor [°C]
CLDS: integrated error signal of cold receptor [°C]
D: heat exchange by conduction [W]
DILAT: vasodilation signal [–]
E: evaporative heat loss at skin [W]
E_{max}: maximum evaporative heat loss [W]
Err: error signal [°C]
E_{sw}: evaporative heat loss by sweating [W]
Height: body height [m^2]
I_{cl}: clothing insulation [clo]
L_R: Lewis ratio (=16.5)[K/kPa]
Mbase: heat production by basal metabolism [W]
$Mbase_{all}$: heat production by basal metabolism in whole body [W]
Mbasef: distribution coefficient of heat production by basal metabolism [–]
Mnst: heat production by non-shivering thermogenesis [W]
Mnstf: distribution coefficient of heat production by non-shivering thermogenesis [–]
$SWdif_{sk}$: heat gain by diffuse shortwave solar radiation at the skin [W]
$SWdir_{sk}$: heat gain by direct shortwave solar radiation at the skin [W]
SWEAT: sweating signal [W]
T: body temperature [°C]
T_a: ambient temperature [°C]
T_o: operative temperature [°C]
Tsetpt: setpoint temperature of the body [°C]
Tshiv: threshold of the head core temperature to start shivering [°C]
Weight: body weight [kg]
$Weight_{ra}$: ratio of body weight to standard body weight [–]
Wrm: error signal in the warm receptor [°C]
WRMS: integrated error signal in the warm receptor [°C]
f_{cl}: clothing area factor [–]
f_{dif}: ratio of diffuse solar radiation to global radiation [–]
f_{eff}: effective radiation factor [–]
f_p: projected area factor [–]
h_c: convective heat transfer coefficient [W/m^2/K]
h_{et}: total evaporative heat transfer coefficient [W/m^2/kPa]
h_r: radiative heat transfer coefficient [W/m^2/K]
h_t: total heat transfer coefficient [W/m^2/K]
i_{cl}: clothing vapor permeation efficiency [–]
p_a: water vapor pressure in the ambient air [kPa]
p_{ssk}: saturated water vapor pressure at the skin temperature [kPa]
ρ_{sk}: solar absorptance of the skin [–]
t: time [s]
τ_{cl}: solar transmittance of clothing [–]
w: skin wettedness [–]

Subscripts
ar: artery
ava: arteriovenous anastomoses (AVA)
cb: central blood
cr: core
fat: fat
i: body segment
j: body tissue
ms: muscle
sk: skin
sve: superficial vein
ve: vein
x: body tissue
x': adjacent body tissue to upstream of blood flow

flow heat exchange in the limbs and improved the prediction accuracy of core and skin temperatures. Smith's model [17], a distributed parameter model, details the vascular system based on Stolwijk's model and determines the heat transfer in a body via the finite element method. Subsequently, models by Takemori et al. [18] and Fu [19] were proposed based on Smith's model. Takemori's AVA model [18] incorporates the arteriovenous anastomoses (AVA) blood flow control and is able to predict local skin

temperatures with higher accuracy than Smith's model [17]. Although the model of Werner and Buse [20] is a distributed parameter model, the shape of the model is not approximated to a cylinder and sphere but based on the actual biological shape of the human body. Thus far, our research team has also developed the 65 multi-node (65MN) [21], joint system thermoregulation model (JOS) [22], and JOS-2 [23] models based on Stolwijk's model. JOS-2 has a blood pool and arteriovenous anastomosis (AVA) blood flow for a detailed simulation of the heat transport due to blood flow.

These models [8,15,16] have been verified only by experiments with subjects mainly aged between 20 and 40. Fiala et al. tested their model by including an experiment with 61 men and women between the ages of 51 and 72 [24]. However, they have not discussed the differences in age [14]. The newly developed JOS-3 model considers the difference in thermo-physiological responses depending on age by adding new parameters to an estimation method for heat production and the decrement of thermoregulations. In addition, we updated the model to improve shivering thermogenesis, a new control method for non-shivering thermogenesis, and the heat gain on the skin due to solar radiation. The newly added or updated equations are as follows: heat gain on the skin by the shortwave solar radiation (Eqs. (14)–(15)), an estimation method for heat production (Eqs. (30)–(32)), aging effects on thermoregulation (Eqs. (33), 44, 45, and 50), and shivering and non-shivering thermogenesis (Eqs. (34)–(39)).

This paper describes all the calculation methods of JOS-3. The validations comparing JOS-2 and JOS-3 concerning heat production and aging effects, and the basic performance of JOS-3 are shown. The model is coded using Python-3, and the package of this model were released in https://github.com/TanabeLab/JOS-3.

2. Body construction

Fig. 1 shows the concept of JOS-3, which is based on Stolwijk's model and derived from JOS-2. JOS-3 consists of the following 85 nodes: the central blood node, 17 artery nodes, 17 vein nodes, 12 superficial vein nodes, 17 core nodes, 2 muscle nodes, 2 fat nodes, and 17 skin nodes. The entire body is divided into the following 17 segments: head, neck, chest, back, pelvis, left (L)-shoulder, L-arm, L-hand, right (R)-shoulder, R-arm, R-hand, L-thigh, L-leg, L-foot, R-thigh, R-leg, and R-foot. The head and pelvis segments have the artery, vein, core, muscle, fat, and skin nodes. The neck chest and back segments have artery, vein, core, and skin nodes. The limb segments have the artery, vein, superficial vein, core, and skin nodes. The artery and vein blood pools are in the center of the core layer, and the superficial vein pool is in the middle of the skin layer. JOS-3 assumes arteriovenous anastomosis (AVA) blood flow in the hand or foot segment that connects the artery to the superficial vein pool. It is assumed that the blood coming from multiple upstream blood flow paths is completely mixed and then flows to downstream tissues in order.

JOS-3 has four layers in the head and pelvis only to maintain sufficient prediction accuracy. In fact, the head does not have a muscle or fat layer like the other parts of the body, but it is described as a thermal layer. Although the layers can be called the first or second layer, we call it muscle and fat for ease of understanding.

3. Heat balance

The heat balance of central blood ($_{cb}$), artery ($_{ar}$), vein ($_{ve}$), superficial vein ($_{sve}$), core ($_{cr}$), muscle ($_{ms}$), fat ($_{fat}$), and skin ($_{sk}$) are expressed in Eqs. (1)–(8). These equations are based on Yokoyama et al. [25,26], Gordon et al. [13], and Mitchell et al. [27]. The central blood exchanges heat with other tissues only by blood flow. In each segment, heat exchange by conduction occurs between a layer and its adjacent layer. In limb segments, additionally, heat is exchanged by conduction between the artery and vein ($D_{ar\text{-}ve[i]}$), vessels and core ($D_{ar\text{-}cr[i]}$ and $D_{ve\text{-}cr[i]}$), and superficial vein and skin ($D_{sve\text{-}sk[i]}$). Heat loss by respiration (RES) occurs in the core chest layer.

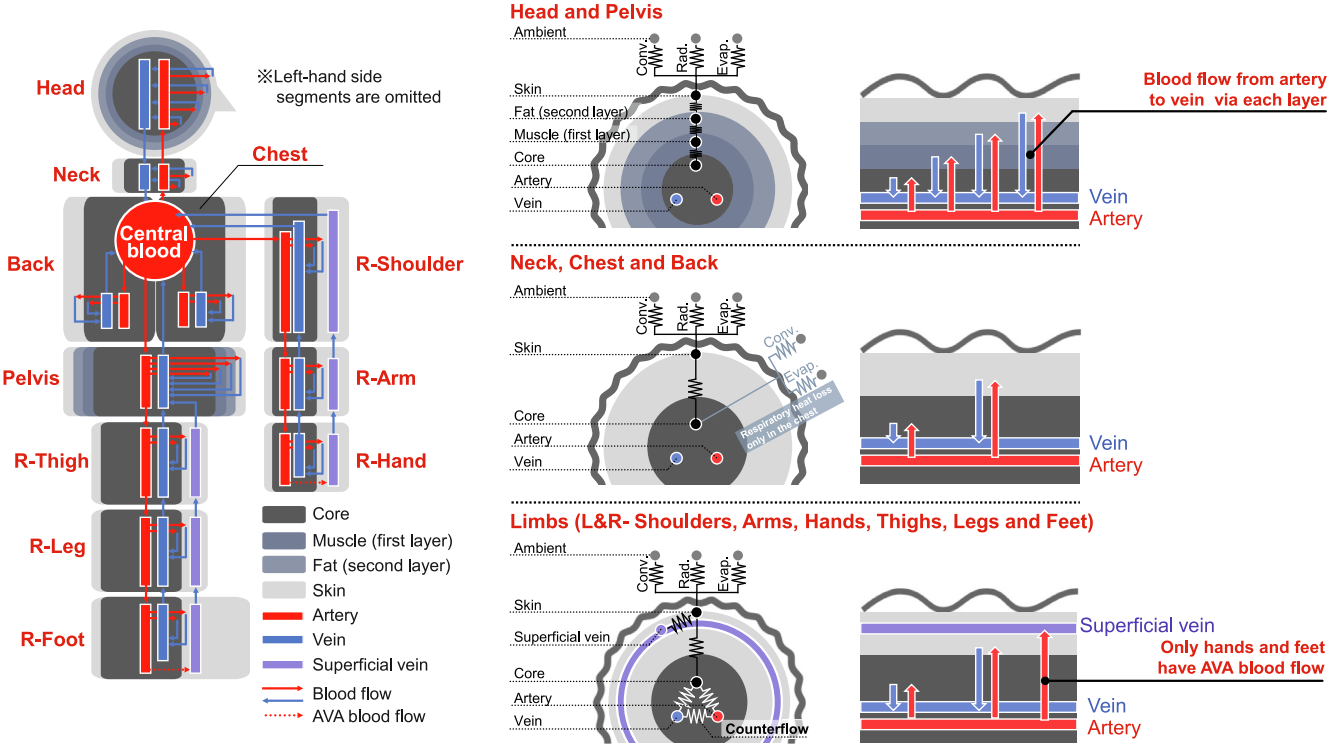

Fig. 1. Concept of JOS-3.

$$Cap_{cb}\frac{dT_{cb}}{dt} = B_{cb} \tag{1}$$

$$Cap_{ar[i]}\frac{dT_{ar[i]}}{dt} = B_{ar[i]} - D_{ar-cr[i]} - D_{ar-ve[i]} \tag{2}$$

$$Cap_{ve[i]}\frac{dT_{ve[i]}}{dt} = B_{ve[i]} - D_{ve-cr[i]} + D_{ar-ve[i]} \tag{3}$$

$$Cap_{sve[i]}\frac{dT_{sve[i]}}{dt} = B_{sve[i]} - D_{sve-sk[i]} \tag{4}$$

$$Cap_{cr[i]}\frac{dT_{cr[i]}}{dt} = \begin{cases} Q_{cr[i]} + B_{cr[i]} - D_{cr-ms[i]} & \text{(HeadandPelvis)} \\ Q_{cr[2]} + B_{cr[2]} - D_{cr-sk[2]} - RES & \text{(Chest)} \\ Q_{cr[i]} + B_{cr[i]} - D_{cr-sk[i]} & \text{(NeckandBack)} \\ Q_{cr[i]} + B_{cr[i]} + D_{ar-cr[i]} + D_{ve-cr[i]} - D_{cr-sk[i]} & \text{(Limbsegments)} \end{cases} \tag{5}$$

$$Cap_{ms[i]}\frac{dT_{ms[i]}}{dt} = Q_{ms[i]} + B_{ms[i]} + D_{cr-ms[i]} - D_{ms-fat[i]} \quad \text{(HeadandPelvis)} \tag{6}$$

$$Cap_{fat[i]}\frac{dT_{fat[i]}}{dt} = Q_{fat[i]} + B_{fat[i]} + D_{ms-fat[i]} - D_{fat-sk[i]} \quad \text{(HeadandPelvis)} \tag{7}$$

$$Cap_{sk[i]}\frac{dT_{sk[i]}}{dt} = \begin{cases} Q_{sk[0]} + B_{sk[0]} + D_{fat-sk[0]} - (C_{[0]} + R_{[0]}) - E_{[0]} + SW_{sk[0]} & \text{(HeadandPelvis)} \\ Q_{sk[i]} + B_{sk[i]} + D_{cr-sk[i]} - (C_{[i]} + R_{[i]}) - E_{[i]} + SW_{sk[i]} & \text{(Neck, ChestandBack)} \\ Q_{sk[i]} + B_{sk[i]} + D_{cr-sk[i]} + D_{sve-sk[i]} - (C_{[i]} + R_{[i]}) - E_{[i]} + SW_{sk[i]} & \text{(Limbsegments)} \end{cases} \tag{8}$$

where $Cap_{j[i]}$ is heat capacity, $T_{j[i]}$ is temperature, t is time, $B_{j[i]}$ is heat exchange by blood, $Q_{j[i]}$ is heat production, $D_{j[i]}$ is heat exchange by conduction, $C_{[i]} + R_{[i]}$ is sensible heat loss from skin, $E_{[i]}$ is the latent heat loss from the skin, and $SW_{sk[i]}$ is the heat gain by shortwave solar radiation at the skin.

4. Boundary conditions

The sensible heat loss from the skin ($C_{[i]} + R_{[i]}$) is expressed in Eqs. (9) and (10), the latent heat loss at the skin ($E_{[i]}$) is expressed in Eqs. (11) and (12), and the heat loss by respiration (RES) is expressed in Eq. (13). The convective heat transfer coefficient (h_c) and the radiative heat transfer coefficient (h_r) were measured by a thermal manikin. Their default values for sitting, standing, and supine postures were set to JOS-3 based on previous studies [28,29]. The total evaporative heat transfer coefficient was calculated using the Lewis ratio (L_R), which was 16.5 K/kPa in this study. Skin wettedness ($w_{[i]}$) is 0.06 in a thermally neutral environment as insensible diffusion. RES is calculated as a function of the total heat produced by the body.

$$C_{[i]} + R_{[i]} = h_{t[i]} \cdot (T_{sk[i]} - T_{o[i]}) \cdot BSA_{[i]} \tag{9}$$

$$\frac{1}{h_{t[i]}} = 0.155 \cdot I_{cl[i]} + \frac{1}{f_{cl[i]} \cdot (h_{c[i]} + h_{r[i]})} \tag{10}$$

$$E_{[i]} = w_{[i]} \cdot h_{et[i]} \cdot (P_{ssk[i]} - P_{a[i]}) \cdot BSA_{[i]} \tag{11}$$

$$\frac{1}{h_{et[i]}} = \frac{0.155 \cdot I_{cl[i]}}{L_R \cdot i_{cl[i]}} + \frac{1}{f_{cl[i]} \cdot L_R \cdot h_{c[i]}} \tag{12}$$

$$RES = \left\{0.0014 \cdot (34 - T_{a[0]}) + 0.0173 \cdot \left(5.87 - p_{a[0]}\right)\right\} \cdot \sum_{i=0}^{16} (Q_{cr[i]} + Q_{ms[i]} + Q_{fat[i]} + Q_{sk[i]}) \tag{13}$$

In JOS-3, the heat exchange of shortwave and longwave solar radiation is calculated separately. The solar radiation is separated into direct and diffuse categories using the method of Reindle et al. [30]. Subsequently, the radiation temperature is calculated from only longwave radiation based on Watanabe et al. [31]. The heat gain by shortwave solar radiation at the skin ($SW_{sk[i]}$) is expressed in Eqs. (14)–(16) and calculated separately for direct ($SWdir_{sk}$) and diffuse ($SWdif_{sk}$) categories. $SWdir_{sk}$ and $SWdif_{sk}$ are calculated from the solar transmittance of clothing ($\tau_{cl[i]}$), solar absorptance of the skin ($\rho_{sk[i]}$), ratio of diffuse to total solar radiation (f_{dif}), projected area factor ($f_{p[i]}$), effective radiation factor ($f_{eff[i]}$), and downward and upward horizontal shortwave radiations (SW_{dw} and SW_{up}), which are measured by the albedometer.

$$SW_{sk[i]} = SWdir_{sk[i]} + SWdif_{sk[i]} \tag{14}$$

$$SWdir_{sk[i]} = \tau_{cl[i]} \cdot \rho_{sk[i]} \cdot f_{p[i]} \cdot (1 - f_{dif}) \cdot SW_{dw} \cdot BSA_{[i]} \tag{15}$$

$$SWdif_{sk[i]} = \tau_{cl[i]} \cdot \rho_{sk[i]} \cdot f_{eff[i]} \cdot \frac{f_{dif} \cdot SW_{dw} + SW_{up}}{2} \cdot BSA_{[i]} \tag{16}$$

5. Physiological parameters

The whole body surface area (BSA_{all}) and the ratio of BSA and $Weight$ to the standard body (BSA_{ra} and $Weight_{ra}$) are expressed in Eqs. (17)–(20). BSA_{all} is calculated from the DuBois equation [32]. BSA_{ra} and $Weight_{ra}$ are the ratios of body surface area and weight to the standard (1.87 m^2 and 74.43 kg, respectively). The local body surface area ($BSA_{[i]}$) is calculated from its standard value ($BSA_{st[i]}$) and ratio (BSA_{ra}), and it is expressed in Eq. (20).

$$BSA_{all} = 0.202 \cdot Weight^{0.425} \cdot Height^{0.725} \tag{17}$$

$$BSA_{ra} = BSA_{all}/1.87 \tag{18}$$

$$Weight_{ra} = Weight/74.43 \tag{19}$$

$$BSA_{[i]} = BSA_{ra} \cdot BSA_{st[i]} \tag{20}$$

The heat capacity ($Cap_{j[i]}$) is expressed in Eq. (21) from the standard body ($Cap_{st,j[i]}$) shown in Table 1. BFB_{ra} is the ratio of the basal blood flow rate to the standard body and is described in chapter 8. The specific heat of individual tissues is assumed as follows: 2.088 kJ/kg/K for bone, 2.506 kJ/kg/K for fat, and 3.758 kJ/kg/K for other tissues, including skin, muscle, viscera, and connective tissues. JOS-3 is composed of 15% bone, 15% fat, and 70% of other structures of the total body weight based on the study by Stolwijk [8]. Stolwijk's model or 65MN do not have nodes for the artery, vein, and superficial vein. Therefore, the heat capacity for the core was subtracted from the blood pools when the thermoregulation model was updated from 65MN to JOS series. The blood volume in the central blood node is assumed to be 2.5 L.

$$Cap_{j[i]} = \begin{cases} Weight_{ra} \cdot Cap_{st,j[i]} & \text{(Layers)} \\ BFB_{ra} \cdot Cap_{st,j[i]} & \text{(Bloodpools)} \end{cases} \tag{21}$$

The heat exchange by conduction between layers and vessels ($D_{j\text{-}j'[i]}$) and heat conductance ($Cdt_{j\text{-}j'[i]}$) are expressed in Eqs. (22) and (23), respectively. Table 2 shows the heat conductance of the

Table 1
Body surface area and heat capacity of the standard body. $Cap_{st,cb}$, $Cap_{st,ms[0]}$, $Cap_{st,fat[0]}$, $Cap_{st,ms[4]}$, and $Cap_{st,fat[4]}$ are 7.196, 0.930, 0.620, 26.672, and 7.011 kJ/K, respectively. The data were derived from Stolwijk [8] and JOS-2 [23].

i	Segment	BSA_{st} [m^2]	$Cap_{st,ar}$ [kJ/K]	$Cap_{st,ve}$ [kJ/K]	$Cap_{st,sve}$ [kJ/K]	$Cap_{st,cr}$ [kJ/K]	$Cap_{st,sk}$ [kJ/K]
0	Head	0.110	0.346	1.156	–	6.202	0.679
1	Neck	0.029	0.090	0.306	–	2.030	0.209
2	Chest	0.175	0.432	1.526	–	37.071	1.588
3	Back	0.161	0.400	1.404	–	33.817	1.462
4	Pelvis	0.221	0.954	2.995	–	16.119	2.002
5	L-Shoulder	0.096	0.067	0.166	0.090	6.118	0.454
6	L-Arm	0.063	0.033	0.086	0.054	4.035	0.302
7	L-Hand	0.050	0.016	0.036	0.040	0.553	0.317
8	R-Shoulder	0.096	0.067	0.166	0.090	6.118	0.454
9	R-Arm	0.063	0.033	0.086	0.054	4.035	0.302
10	R-Hand	0.050	0.016	0.036	0.040	0.553	0.317
11	L-Thigh	0.209	0.293	0.745	0.266	19.122	1.202
12	L-Leg	0.112	0.144	0.360	0.180	10.321	0.608
13	L-Foot	0.056	0.037	0.086	0.076	0.755	0.385
14	R-Thigh	0.209	0.293	0.745	0.266	19.122	1.202
15	R-Leg	0.112	0.144	0.360	0.180	10.321	0.608
16	R-Foot	0.056	0.037	0.086	0.076	0.755	0.385

Table 2
Heat conductance of the standard body. The head and pelvis consist of core, muscle, fat, and skin layers. Thus, the numbers in the $Cdt_{st,cr\text{-}sk}$ column of the head and pelvis rows means $Cdt_{st,cr\text{-}ms}$, $Cdt_{st,ms\text{-}fat}$, and $Cdt_{st,fat\text{-}sk}$. The data were derived from Stolwijk [8] and JOS-2 [23].

i	Segment	$Cdt_{st,ar\text{-}cr}$ and $Cdt_{st,ve\text{-}cr}$ [W/K]	$Cdt_{st,sve\text{-}sk}$ [W/K]	$Cdt_{st,ar\text{-}ve}$ [W/K] (countercurrent)	$Cdt_{st,cr\text{-}sk}$ [W/K] ($Cdt_{st,cr\text{-}ms}$, $Cdt_{st,ms\text{-}fat}$, $Cdt_{st,fat\text{-}sk}$)
0	Head	–	–	–	(1.60, 13.20, 16.00)
1	Neck	–	–	–	0.91
2	Chest	–	–	–	1.79
3	Back	–	–	–	1.64
4	Pelvis	–	–	–	(3.08, 10.37, 41.50)
5	L-Shoulder	0.59	57.74	0.54	1.50
6	L-Arm	0.38	37.77	0.35	0.98
7	L-Hand	1.53	16.63	0.76	2.18
8	R-Shoulder	0.59	57.74	0.54	1.50
9	R-Arm	0.38	37.77	0.35	0.98
10	R-Hand	1.53	16.63	0.76	2.18
11	L-Thigh	0.81	102.01	0.83	2.47
12	L-Leg	0.44	54.78	0.44	1.33
13	L-Foot	1.82	24.28	0.99	3.37
14	R-Thigh	0.81	102.01	0.83	2.47
15	R-Leg	0.44	54.78	0.44	1.33
16	R-Foot	1.82	24.28	0.99	3.37

standard body. $Cdt_{j\text{-}j'[i]}$ is variable by the body surface area and weight; however, the head and neck are defined as a sphere and not a cylinder. Therefore, the following two equations are used:

$$D_{j-j'_{[i]}} = Cdt_{j-j'[i]} \cdot \left(T_{j[i]} - T_{j'[i]}\right) \tag{22}$$

$$Cdt_{j-j'[i]} = \begin{cases} \left(Weight_{ra}/BSA_{ra}\right) \cdot Cdt_{st,j-j'[i]} & (\text{HeadandNeck}) \\ \left(BSA_{ra}{}^2/Weight_{ra}\right) \cdot Cdt_{st,j-j'[i]} & (\text{Othersegments}) \end{cases} \tag{23}$$

6. Error signals

Error signals for body segments and integrated signals are expressed in Eqs. (24)–(28). Table 3 shows the setpoint temperatures of body segments ($T_{setpt,j,[i]}$) and the distribution coefficients of thermal receptors ($SKINR_{[i]}$). $SKINR_{[i]}$ is divided values based on Stolwijk's study [8] according to the size of the body surface area. $T_{setpt,j,[i]}$ is defined as the body temperature of the model that does not have a thermoregulation system (only a passive system) under thermal neutral operative temperature, based on the PMV-model [1] (relative humidity = 50%, air velocity = 0.10 m/s, PAR = 1.25, and whole clothing insulation = 0.0 clo).

$$Err_{j[i]} = T_{j[i]} - T_{setpt,j[i]} \tag{24}$$

$$Wrm_{[i]} = \begin{cases} 0 & (Err_{sk[i]} \le 0) \\ Err_{sk[i]} & (Err_{sk[i]} > 0) \end{cases} \tag{25}$$

Table 3
Setpoint temperature of body segments and distribution coefficient of thermal receptor. $T_{setpt,j,[i]}$ are analyzed values of JOS-3 and SKINR were derived from Stolwijk [8] and JOS-2 [23].

i	Segment	$T_{setpt,cr}$ [°C]	$T_{setpt,sk}$ [°C]	$SKINR$ [–]
0	Head	37.46	35.13	0.055
1	Neck	37.00	35.26	0.014
2	Chest	37.23	34.76	0.149
3	Back	37.29	34.67	0.132
4	Pelvis	37.50	34.92	0.212
5	L-Shoulder	36.41	34.39	0.023
6	L-Arm	35.87	33.99	0.012
7	L-Hand	35.05	34.44	0.092
8	R-Shoulder	36.41	34.39	0.023
9	R-Arm	35.87	33.99	0.012
10	R-Hand	35.05	34.44	0.092
11	L-Thigh	36.84	34.28	0.050
12	L-Leg	36.48	34.08	0.025
13	L-Foot	34.74	34.24	0.017
14	R-Thigh	36.84	34.28	0.050
15	R-Leg	36.48	34.08	0.025
16	R-Foot	34.74	34.24	0.017

$$Cld_{[i]} = \begin{cases} -Err_{sk[i]} & (Err_{sk[i]} \le 0) \\ 0 & (Err_{sk[i]} > 0) \end{cases} \quad (26)$$

$$WRMS = \sum_{i=0}^{16} SKINR_{[i]} \cdot Wrm_{[i]} \quad (27)$$

$$CLDS = \sum_{i=0}^{16} SKINR_{[i]} \cdot Cld_{[i]} \quad (28)$$

7. Heat production

It is known that non-shivering thermogenesis (NST) by brown adipose tissue (BAT) occurs when a human is exposed to cold temperatures, causing seasonal effects [33,34]. JOS-3 considers non-shivering thermogenesis and physiological functional changes by acclimation to colder temperatures, and mild cold temperature control of shivering [35]. The heat production ($Q_{j[i]}$) is expressed by Eq. (29), and it is defined as the sum of heat production (Table 4) by the basal metabolic rate ($Mbase_{j[i]}$), work ($Mwork_{[i]}$), shivering ($Mshiv_{[i]}$), and non-shivering ($Mnst_{[i]}$). $Mwork_{[i]}$, $Mshiv_{[i]}$, and $Mnst_{[i]}$ are produced in the core layers of all segments, excluding the head. $Mwork_{[0]}$, $Mshiv_{[0]}$, and $Mnst_{[0]}$ are produced in the muscle of the head.

$$Q_{j[i]} = Mbase_{j[i]} + Mwork_{[i]} + Mshiv_{[i]} + Mnst_{[i]} \quad (29)$$

7.1. Basal metabolic rate and external work

The basal metabolic rate and metabolic rate required by work are expressed in Eqs. (30)–(32) using the Harris–Benedict model [36,37], which varies according to body weight, height, age, and sex. Table 5 shows the physical activity ratio (*PAR*) of typical indoor activities [38], by which the heat production of work is calculated with.

$$Mbase_{all} = \begin{cases} (88.362 + 500.3 \cdot Height + 13.397 \cdot Weight - 5.677 \cdot Age) \cdot 0.048 & \text{(Male)} \\ (447.593 + 479.9 \cdot Height + 9.247 \cdot Weight - 4.330 \cdot Age) \cdot 0.048 & \text{(Female)} \end{cases} \quad (30)$$

$$Mbase_{j[i]} = Mbasef_{j[i]} \cdot Mbase_{all} \quad (31)$$

$$Mwork_{[i]} = Mworkf_{[i]} \cdot (PAR - 1) \cdot Mbase_{all} \quad (32)$$

Table 5
PAR of typical indoor activities. The data is based on FAO [38].

Activity level	Male	Female
Sleeping	1.0	1.0
Lying	1.2	1.2
Sitting quietly	1.2	1.2
Standing	1.4	1.5
Eating and drinking	1.4	1.6
Writing	1.4	1.4
Walking slowly	2.8	3.0
Walking quickly	3.8	–
Climbing stairs	5.0	–

7.2. Shivering thermogenesis

The heat production by shivering is expressed in Eqs. (33)–(35). JOS-2 tends to overestimate heat production under mild cold conditions. Moreover, shivering thermogenesis begins after non-shivering thermogenesis. We added new controls for restraining the increment of shivering thermogenesis and delaying its start in the model. In JOS-3, the variation of the integrated error signal of shivering (*SHIV*) per time is limited to 0.0077 W/s, based on human experiments [40]. In addition, to delay the start of shivering, JOS-3 has the threshold of the head core temperature to start shivering (*Tshiv*). *Tshiv* is expressed in Eq. (35) from the relationship between *Tshiv* and mean skin temperature ($T_{sk,whole}$) [41]. In this study, the upper limit of *Tshiv* was set to 36.6 °C [42]. Furthermore, the aging factor (*AGshiv*) of shivering thermogenesis was added to the model. *AGshiv* is shown in Table 6. It is assumed that the decrease in shivering with aging is proportional to the decrease in the basal metabolic rate with aging. *AGshiv* is defined based on the Harris–Benedict equation [36].

$$Mshiv_{[i]} = Mshivf_{[i]} \cdot AGshiv \cdot BSA_{ra} \cdot SHIV \quad (33)$$

$$SHIV = 24.36 \cdot Cld_{cr[0]} \cdot CLDS \quad (34)$$

$$Tshiv = \begin{cases} -0.24 \cdot T_{sk,whole} + 44.10 & \text{(Male)} \\ -0.23 \cdot T_{sk,whole} + 43.05 & \text{(Female)} \end{cases} \quad (35)$$

7.3. Non-shivering thermogenesis (NST)

The heat production by non-shivering ($Mnst_{[i]}$) is expressed in Eqs. (36)–(39). NST is produced by BAT and organs. In this study,

Table 4
Distribution coefficients of basal metabolism, work, shivering and non-shivering thermogenesis. $Mbasef_{ms[0]}$, $Mbasef_{fat[0]}$, $Mbasef_{ms[4]}$, and $Mbasef_{fat[4]}$, are 0.252, 0.127, 4.804, and 0.950 [$\times 10^{-2}$], respectively. Only *Mnstf* is based on the study by Matsumura et al. [39]. The other values were derived from Stolwijk [8] and JOS-2 [23].

i	Segment	$Mbasef_{cr}$ [$\times 10^{-2}$]	$Mbasef_{sk}$ [$\times 10^{-2}$]	*Mworkf* [–]	*Mshivf* [–]	*Mnstf* [–]
0	Head	19.551	0.152	–	0.034	–
1	Neck	0.324	0.033	–	0.044	0.190
2	Chest	28.689	0.211	0.091	0.274	–
3	Back	25.677	0.187	0.080	0.242	0.190
4	Pelvis	9.609	0.300	0.129	0.388	0.190
5	L-Shoulder	1.435	0.059	0.026	0.002	0.215
6	L-Arm	0.409	0.031	0.014	0.001	–
7	L-Hand	0.106	0.059	0.005	–	–
8	R-Shoulder	1.435	0.059	0.026	0.002	0.215
9	R-Arm	0.409	0.031	0.014	0.001	–
10	R-Hand	0.106	0.059	0.005	–	–
11	L-Thigh	1.557	0.144	0.201	0.004	–
12	L-Leg	0.422	0.027	0.099	0.002	–
13	L-Foot	0.250	0.118	0.005	–	–
14	R-Thigh	1.557	0.144	0.201	0.004	–
15	R-Leg	0.422	0.027	0.099	0.002	–
16	R-Foot	0.250	0.118	0.005	–	–

the upper limit of the non-shivering signal (*NSTmax*) is defined by the amount of BAT available. The upper limit for NST from an organ in the standard body of JOS-3 is 15.04 W [43]. The volume of BAT (*BAT*) is defined by the BMI, aging factor of the BAT volume (*AGbat*), aging factor of the BAT incidence (*AGbatinc*), and the condition of cold acclimation [34,43]. A previous study indicated that BAT activity was not present in all individuals [34]. Moreover, it was reported that the incidence of BAT activity decreased with age, and individuals aged 60 years or older had almost no BAT activity [43]. In this study, the aging factor of the BAT incidence (*AGbatinc*) is directly introduced into the coefficients to calculate the volume of BAT and is expressed as Eq. (39). Therefore, this method facilitates the estimation of the average BAT volume of people, but it is difficult to apply for individual estimation.

$$Mnst_{[i]} = BSA_{ra} \cdot Mnstf_{[i]} \cdot NST \tag{36}$$

$$NST = \min(2.8 \cdot CLDS, NSTmax) \tag{37}$$

$$NSTmax = 3.36 \cdot BAT + 15.04 \tag{38}$$

$$BAT = \begin{cases} AGbat \cdot AGbatinc \cdot 10^{(-0.11 \cdot BMI + 2.77)} & \text{(Nomal)} \\ AGbat \cdot AGbatinc \cdot (10^{(-0.11 \cdot BMI + 2.77)} + 3.46) & \text{(Coldacclimated)} \end{cases} \tag{39}$$

8. Vasodilation and vasoconstriction

8.1. Basal blood flow

The heat transfer by blood flow (B_x) is expressed in Eq. (40) by the sum of the blood flow of upstream tissues and the temperature difference between tissues. The subscript *x'* defines adjacent layers or blood pools of the upstream tissues, and $BF_{x'-x}$ is the blood flow rate from *x'* to *x*.

$$B_x = \sum 1.067\hat{A} \cdot BF_{x'-x} \cdot (T_{x'} - T_x) \tag{40}$$

The blood flow rate of layers $BF_{j[i]}$ is expressed in Eqs. (41)–(44). The blood flow rate in the muscle or core layers depends on heat production. It is assumed that a 1 L/h blood flow rate is required to increase the metabolism by 1.163 W. BFB_{ra} is the ratio of basal blood flow rate to the standard (290 L/h). The aging factor of the cardiac index *(AGci)* is shown in Table 8 based on the study by Strehler [44].

$$BF_{j[i]} = BFB_{j[i]} + (Mwork_{[i]} + Mshiv_{[i]} + Mnshiv_{[i]})/1.163 \tag{41}$$

$$BFB_{j[i]} = BFB_{ra} \cdot BFB_{st,j[i]} \tag{42}$$

$$BFB_{ra} = BFB_{all}/290 \tag{43}$$

$$BFB_{all} = CI \cdot AGci \cdot 60 \cdot BSA_{all} \tag{44}$$

8.2. Skin blood flow

The skin blood flow rate ($BF_{sk[i]}$) is expressed in Eqs. (45)–(47). Unlike JOS-2, the vasodilation signal is dimensionless in JOS-3, but the vasodilation control of JOS-3 is the same as that of JOS-2. $AG_{dilat[i]}$ and $AG_{stric[i]}$ are aging factors of vasodilation and vasoconstriction in each segment. The vasodilator response is said to decay with age. In this study, $AG_{dilat[i]}$ and $AG_{stric[i]}$ are defined as 1.0 [-] in all segments, but only $AG_{dilat[i]}$ for ages over 60 years is defined, as indicated in Table 7, which is based on the study by Inoue et al. [45].

$$BF_{sk[i]} = \frac{1.0 + SKIND_{[i]} \cdot AGdilat_{[i]} \cdot DILAT}{1.0 + SKINC_{[i]} \cdot AGstric_{[i]} \cdot STRIC} \cdot BFB_{sk[i]} \cdot 2.0^{\frac{Err_{sk[i]}}{6}} \tag{45}$$

$$DILAT = 100.5 \cdot Err_{cr[0]} + 6.4 \cdot (WRMS - CLDS) \tag{46}$$

$$STRIC = -10.8 \cdot Err_{cr[0]} - 10.8 \cdot (WRMS - CLDS) \tag{47}$$

8.3. Arteriovenous anastomosis (AVA) blood flow

The AVA blood flow rate ($BF_{ava[i]}$) is expressed in Eqs. (48) and (49), based on the study by Takemori et al. [18]. $O_{ava[i]}$ is the openness rate of AVA, and a value between 0 and 1. $T_{ct,body}$ and $T_{setpt,ct,-}$

Table 6
Aging factor of shivering and non-shivering. *AGshiv* is a calculated value with Harris–Benedict equation [36]. *AGbat* and *AGbatinc* are based on the study by Yoneshiro et al. [43].

Age	*AGshiv* [–]	*AGbat* [–]	*AGbatinc* [–]
20 s	1.00	1.61	0.53
30 s	0.96	1.00	0.39
40 s	0.93	0.80	0.27
50 s	0.89	0.80	0.13
60 s	0.85	0.80	0.00

Table 7
Basal blood flow rate of the standard body and coefficients of skin blood flow. $BFB_{st,ms[0]}$, $BFB_{st,fat[0]}$, $BFB_{st,ms[4]}$, and $BFB_{st,fat[4]}$ are 0.68, 0.27, 12.61, and 2.23 L/h, respectively. Only *AGdilat* is based on the study by Inoue et al. [45]. The other values were derived from Stolwijk [8] and JOS-2 [23].

i	Segment	$BFB_{st,cr}$ [L/h]	$BFB_{st,cr}$ [L/h]	*SKIND* [–]	*SKINC* [–]	*AGdilat* [–] (Age > 60)
0	Head	35.25	1.75	0.070	0.022	0.91
1	Neck	15.24	0.33	0.099	0.022	0.91
2	Chest	89.21	1.97	0.058	0.064	0.47
3	Back	87.66	1.48	0.068	0.064	0.47
4	Pelvis	18.67	2.27	0.071	0.064	0.31
5	L-Shoulder	1.81	0.91	0.040	0.021	0.47
6	L-Arm	0.94	0.51	0.037	0.021	0.47
7	L-Hand	0.22	1.11	0.063	0.149	0.47
8	R-Shoulder	1.81	0.91	0.040	0.021	0.47
9	R-Arm	0.94	0.51	0.037	0.021	0.47
10	R-Hand	0.22	1.11	0.063	0.149	0.47
11	L-Thigh	1.41	1.46	0.074	0.021	0.31
12	L-Leg	0.16	0.65	0.041	0.021	0.31
13	L-Foot	0.08	0.93	0.062	0.149	0.31
14	R-Thigh	1.41	1.46	0.074	0.021	0.31
15	R-Leg	0.16	0.65	0.041	0.021	0.31
16	R-Foot	0.08	0.93	0.062	0.149	0.31

$_{body}$ are the weighted average temperatures of the heat capacity for the chest, back, and pelvis cores.

$$BF_{ava[i]} = \begin{cases} 1.71 \cdot BFB_{ra} \cdot O_{ava[i]} & \text{(Hand)} \\ 2.16 \cdot BFB_{ra} \cdot O_{ava[i]} & \text{(Foot)} \end{cases} \quad (48)$$

$$O_{ava[i]} = \begin{cases} 0.265 \cdot \{T_{sk,whole} - (T_{setpt,sk,whole} - 0.43)\} + 0.953 \cdot \{T_{cr,body} - (T_{setpt,cr,body} - 0.1905)\} + 0.9126 & \text{(Hand)} \\ 0.265 \cdot \{T_{sk,whole} - (T_{setpt,sk,whole} + 0.997)\} + 0.953 \cdot \{T_{cr,body} - (T_{setpt,cr,body} - 0.0095)\} + 0.9126 & \text{(Foot)} \end{cases} \quad (49)$$

9. Sweating

Evaporative heat loss by sweating ($E_{sw[i]}$) is expressed in Eqs. (50)–(52). When skin wettedness ($w_{[i]}$) increases, sweat drops from the body and becomes ineffective at cooling. It has been reported that $w_{[i]}$ did not exceed the value between 0.7 and 1.0 by Gagge et al. [7]. Thus, JOS-3 has the upper limit of $w_{[i]}$ between 0.7 and 1.0. The human body has an eccrine sweat gland that contributes to thermogenic sweating, and an apocrine sweat gland that contributes to psychogenic sweating. JOS-2's distribution coefficient of sweating (*SKINS*), which is based on Stolwijk's model [8], is defined based on anatomical data obtained by measuring the number of sweat glands on the cadaver. In JOS-3, *SKINS* (Table 9) is redefined by Kuno [46]. The aging factor of sweating (*AGsweat*) is typically defined as 1.0 in all segments and changed for ages over 60 years, based on the study by Inoue et al. [45].

$$E_{sw[i]} = SKINS_{[i]} \cdot AGsweat_{[i]} \cdot SWEAT \cdot BSA_{ra} \cdot 2^{\frac{Err_{sk[i]}}{10}} \quad (50)$$

Table 8
Aging factor of cardiac index. The data are based on the study by Strehler [44].

Age	*AGci* [–]
20–40 s	1.00
50 s	0.85
60 s	0.75
70 s-	0.70

Table 9
Coefficients of sweating. *SKINS* is based on the study by Kuno [46] and *AGsweat* is based on the study by Inoue et al. [45].

i	Segment	*SKINS* [–]	*AGsweat* [–] (Age > 60)
0	Head	0.064	0.69
1	Neck	0.017	0.69
2	Chest	0.146	0.59
3	Back	0.129	0.52
4	Pelvis	0.206	0.40
5	L-Shoulder	0.051	0.75
6	L-Arm	0.026	0.75
7	L-Hand	0.016	0.75
8	R-Shoulder	0.051	0.75
9	R-Arm	0.026	0.75
10	R-Hand	0.016	0.75
11	L-Thigh	0.073	0.40
12	L-Leg	0.036	0.40
13	L-Foot	0.017	0.40
14	R-Thigh	0.073	0.40
15	R-Leg	0.036	0.40
16	R-Foot	0.017	0.40

$$SWEAT = 371.2 \cdot Err_{cr[0]} + 33.64 \cdot (WRMS - CLDS) \quad (51)$$

$$w_{[i]} = 0.06 + 0.94 \cdot \frac{E_{sw[i]}}{E_{max[i]}} \quad (52)$$

10. Validation

To validate this model, we simulated the thermo-physiological responses of humans on three kinds of experiments previously conducted by Inoue et al. [47], Werner and Reents [48], and Stolwijk and Hardy [49,50]. In simulating the experiments of Inoue, the effects of changing the estimation method of heat production and physical properties due to aging were analyzed by comparing JOS-2 and JOS-3. The experiments of Werner and Reents and of Stolwijk and Hardy were simulated to measure the basic performance of JOS-3. The experiments of Werner and Reents were performed in seven types of stable environments. Stolwijk and Hardy experiments were carried out in nine types of transient environments.

10.1. Validation of heat production and aging effects by comparing JOS-2 and JOS-3 (Inoue's experiment [45])

In this simulation, we examined the effects of predicted thermal physiological responses by changing the estimation method of heat production and physical properties owing to aging. Inoue et al. [47] measured the metabolic rate and skin temperatures of nine young men and ten older men under two cold conditions. The subjects were dressed only in swimming trunks and seated on a chair in the chamber for 60 min, where the air temperature was controlled at 28 °C. Subsequently, they moved to the other chamber where the operative temperature was controlled at 12 or 17 °C, and the relative humidity was controlled at 45%, and stayed for 60 min.

Table 10 lists the input conditions. The environmental conditions used as the input to the model followed the literature. The input conditions of body composition were set as the average values of nine or ten subjects. The clothing insulations of pelvis and thighs were estimated based on the previous study [51] and were set to 0.6 clo as swimming trunks. The clothing insulation of other parts was set to zero. The heat transfer coefficients were set to the measured values using a thermal manikin in a sitting [28].

Fig. 2 and Table 11 show the comparison of the data from Inoue et al. (EXP) [47] and the predicted data of JOS-2 [23] and JOS-3 for the metabolic rate, rectal temperature, and mean skin temperature. The predicted rectal temperatures were the pelvis core temperatures of JOS-2 and JOS-3. Compared to JOS-2, JOS-3 improved the prediction accuracy of the metabolic rate in all ages and mean skin temperature in the older. By adding a new control method for shivering thermogenesis and non-shivering thermogenesis, the overestimated metabolic rate in JOS-2 decreased. Therefore, the predicted metabolic rate of JOS-3 approached the measured value in all experimental conditions. Conversely, the predicted rectal temperature of JOS-3 decreased due to a decrease in the metabolic rate. Consequently, the mean absolute error (MAE) and root mean-squared error (RMSE) of the rectal temperature were lower in JOS-3 than in JOS-2 under three conditions (Y12, Y17, and O17). Since the rectal temperatures of JOS-3 were higher than those of JOS-2 at the start of the experiment, the differences in setpoint temper-

Table 10
Input conditions to simulate the experiment of Inoue et al. [47].

(a) Experimental schedule.

		Preparation	Chamber
Time	[min]	60	60
Operative temp.	[°C]	28	12 or 17
Relative humidity	[%]	0.1	
Air velocity	[m/s]	45	
Physical activity ratio	[–]	1.2	

(b) Subjects' information. The values are the average and variance of nine young and ten older males.

Subject	Height [m]	Weight [kg]	Age [year]
Young (n = 9)	1.73 (0.02)	64.5 (2.8)	22 (0.5)
Older (n = 10)	1.60 (0.02)	53.8 (1.6)	63 (0.5)

(c) Experimental patterns and symbols.

Symbol	Subject	Operative temp. in chamber
Y12	Young	12 °C
O12	Older	12 °C
Y17	Young	17 °C
O17	Older	17 °C

atures, which were affected by changing the model composition and heat production, are considered the cause of a small improvement in accuracy. For the mean skin temperature, the prediction accuracy of JOS-3 improved under all conditions, compared to JOS-2. In older subjects' conditions, both the MAE and RMSE remarkably decreased by over 0.35 °C. This occurred because of the changes in the cardiac index and physiological properties of sieving heat production owing to aging.

10.2. Validation of the basic performance of the model in constant conditions (Werner and reents' experiment [48])

The purpose of this simulation is to determine the basic performance of JOS-3 under constant conditions. The human experiments by Werner and Reents [48] were carried out at seven different air temperatures (10, 20, 30, 35, 40, 45, and 50 °C) with six male subjects (age: 21–27 years, weight: 74.2 ± 8.1 kg, height: 1.806 ± 0.07 m). The deviation of the surrounding wall temperature and air temperature was less than 1 °C. The relative humidity remained nearly constant at 40 ± 5%, and the air velocity was less than 0.2 m/s. The subjects wore only shorts, laid on a hammock, and were exposed to stable conditions for 120 min at different air temperatures. Rectum and tympanum temperatures were measured as core temperatures, and 12 skin temperatures (forehead, chest, back, abdomen, upper arm, forearm, hand, thigh, calf, foot, and toe) were measured.

Table 12 lists the input conditions. Environmental conditions used for the input of the model followed the literature value. The input conditions of body composition were set as the average values of six male subjects (height: 1.81 m, weight: 74.2 kg, and age: 23 years). The physical activity ratio was assumed to be 1.2. The clothing insulations for pelvis and thighs, considered as shorts, were set to 0.6 clo based on a previous study [51]. The clothing

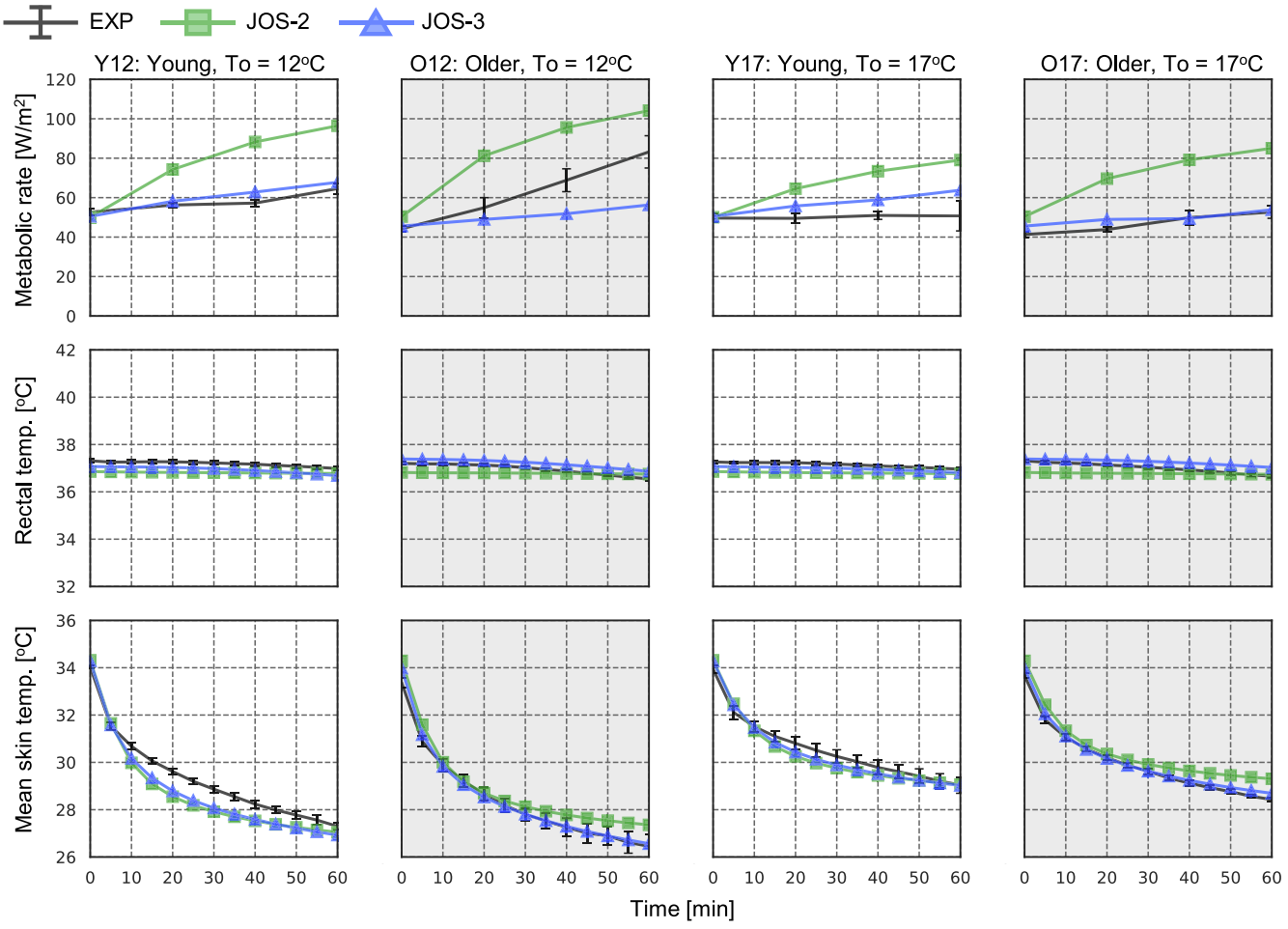

Fig. 2. Comparison of the data from Inoue et al. [47] (EXP) and predicted data (JOS-2 [23] and JOS-3). The width of the error bar of EXP indicates the variance according to Inoue's study.

Table 11
Mean error (ME), standard deviation (SD), mean absolute error (MAE), and root mean-squared error (RMSE) of metabolic rate, rectal temperature, and mean skin temperature between the data from Inoue et al. [47] (EXP) and predicted data (JOS-2 [23] and JOS-3).

			EXP vs JOS-2				EXP vs JOS-3			
Experiment		Data type	ME	SD	MAE	RMSE	ME	SD	MAE	RMSE
Y12: Young	Metabolic rate	[W/m^2]	19.58	16.07	20.87	24.03	2.13	3.25	3.21	3.53
T_o = 12 °C	Rectal temp.	[°C]	−0.38	0.08	0.38	0.38	−0.25	0.03	0.25	0.25
	Mean skin temp.	[°C]	−0.59	0.43	0.65	0.72	−0.52	0.33	0.57	0.61
O12: Older	Metabolic rate	[W/m^2]	20.04	9.63	20.04	21.71	−12.12	12.40	12.79	16.20
T_o = 12 °C	Rectal temp.	[°C]	−0.17	0.21	0.23	0.26	0.24	0.05	0.24	0.25
	Mean skin temp.	[°C]	0.48	0.33	0.48	0.57	0.06	0.20	0.13	0.20
Y17: Young	Metabolic rate	[W/m^2]	16.57	12.06	16.57	19.59	7.01	5.05	7.01	8.26
T_o = 17 °C	Rectal temp.	[°C]	−0.34	0.08	0.34	0.35	−0.17	0.02	0.17	0.17
	Mean skin temp.	[°C]	−0.21	0.32	0.33	0.37	−0.14	0.24	0.25	0.27
O17: Older	Metabolic rate	[W/m^2]	24.13	10.37	24.13	25.75	2.52	2.63	2.76	3.40
T_o = 17 °C	Rectal temp.	[°C]	−0.24	0.19	0.25	0.30	0.24	0.09	0.24	0.26
	Mean skin temp.	[°C]	0.48	0.25	0.48	0.54	0.12	0.12	0.13	0.17

insulation of other parts was set to zero. The effects of the hammock on clothing insulation were not considered in this simulation. The upper limit of $w_{[i]}$ was set to 1.0. Convective heat transfer coefficients (h_c) were calculated using computational fluid dynamics (CFD), scFLOW [23]. Table 12-(b) shows the values of h_c when the air velocity was set to equal 0.3 m/s from the back to the front wall.

Fig. 3 and Table 13 show the comparison between the data of Werner and Reents (EXP) [48] and the predicted data JOS-3 for the rectal, mean skin, and 10 local skin temperatures measured 120 min after entering the chamber under six experimental conditions (operative temperatures were 10, 20, 30, 35, 40, 45, and 50 °C). The predicted rectal temperatures were the pelvis core temperatures of JOS-3. The MAE and RMSE of rectal, mean skin, and 10 local skin temperatures were 0.42–1.31 and 0.50–1.77 °C, respectively. The error in the mean skin temperature was low compared with other segments. In the 10 °C condition, the rectal and seven local skin temperatures were underestimated by JOS-3 compared to EXP. It is considered that reviewing the distribution of heat production and basal blood flow rate improves the prediction accuracy of the model.

10.3. Validation of the basic performance of the model in the transient condition (Stolwijk and Hardy's experiments [49,50])

We simulated Stolwijk and Hardy's experiments [49,50] under nine kinds of step-change conditions for men at rest to examine the basic performance of JOS-3. The subjects were three young males and undressed. They stayed in a climate chamber (operative temperature of 18.0–43.0 °C) for 60 min. Subsequently, they moved and stayed in the other chamber (operative temperatures of 17.0–47.8 °C) for 120 min. They then returned to the first chamber and remained there for 60 min.

Table 14 shows the input conditions; environmental conditions followed literature values in the experiment. Because the subject, AS, is significantly different from the body of the other subjects, the body information was input for the values of the three subjects described in the literature, respectively. The simulation was performed three times under different body compositions, and the average predicted values from the three models were compared with the measured values. From Fig. 1 in [49], it was considered that the skin temperature of the subjects was affected by the thermal resistance of the chair. McCoullough et al.[52] showed that the entire thermal resistance increased by 0.1 to 0.3 clo in sitting a chair. In this study, it was assumed that the clothing insulations of the back, pelvis, both thighs, and legs, which the chair affected as thermal resistance, were set to 0.3 clo. The upper limit of $w_{[i]}$ was set to 1.0. As the initial condition of the model, the model was simulated for 60 min at 28 °C before phase 1. The convective heat transfer coefficients were set to the measured values by a sitting thermal manikin [28].

Fig. 4 and Table 15 show the comparison of the data from Stolwijk and Hardy (EXP) [49,50] and the predicted data JOS-3 for the rectal and mean skin temperatures under nine transient environ-

Table 12
Input conditions to simulate the Werner and Reents' experiment [48].

(a) Experimental schedule

		Preparation	Chamber
Time	[min]	60	120
Operative temp.	[°C]	30	10, 20, 30, 35,40, 45, 50
Mean radiant temp.	[°C]	30	30
Relative humidity	[%]	40	40
Physical activity ratio	[-]	1.2	1.2

(b) Convective heat transfer coefficient [W/K m^2]. The values were calculated by computational fluid dynamics (CFD), scFLOW, and based on the study of Y. Kobayashi et al. [23].

i	Segment	Value	*i*	Segment	Value
0	Head	5.41	9	R-Arm	5.23
1	Neck	5.16	10	R-Hand	8.11
2	Chest	5.17	11	L-Thigh	6.23
3	Back	5.13	12	L-Leg	5.14
4	Pelvis	5.15	13	L-Foot	5.55
5	L-Shoulder	5.18	14	R-Thigh	6.03
6	L-Arm	5.22	15	R-Leg	5.14
7	L-Hand	8.71	16	R-Foot	5.5
8	R-Shoulder	5.17			

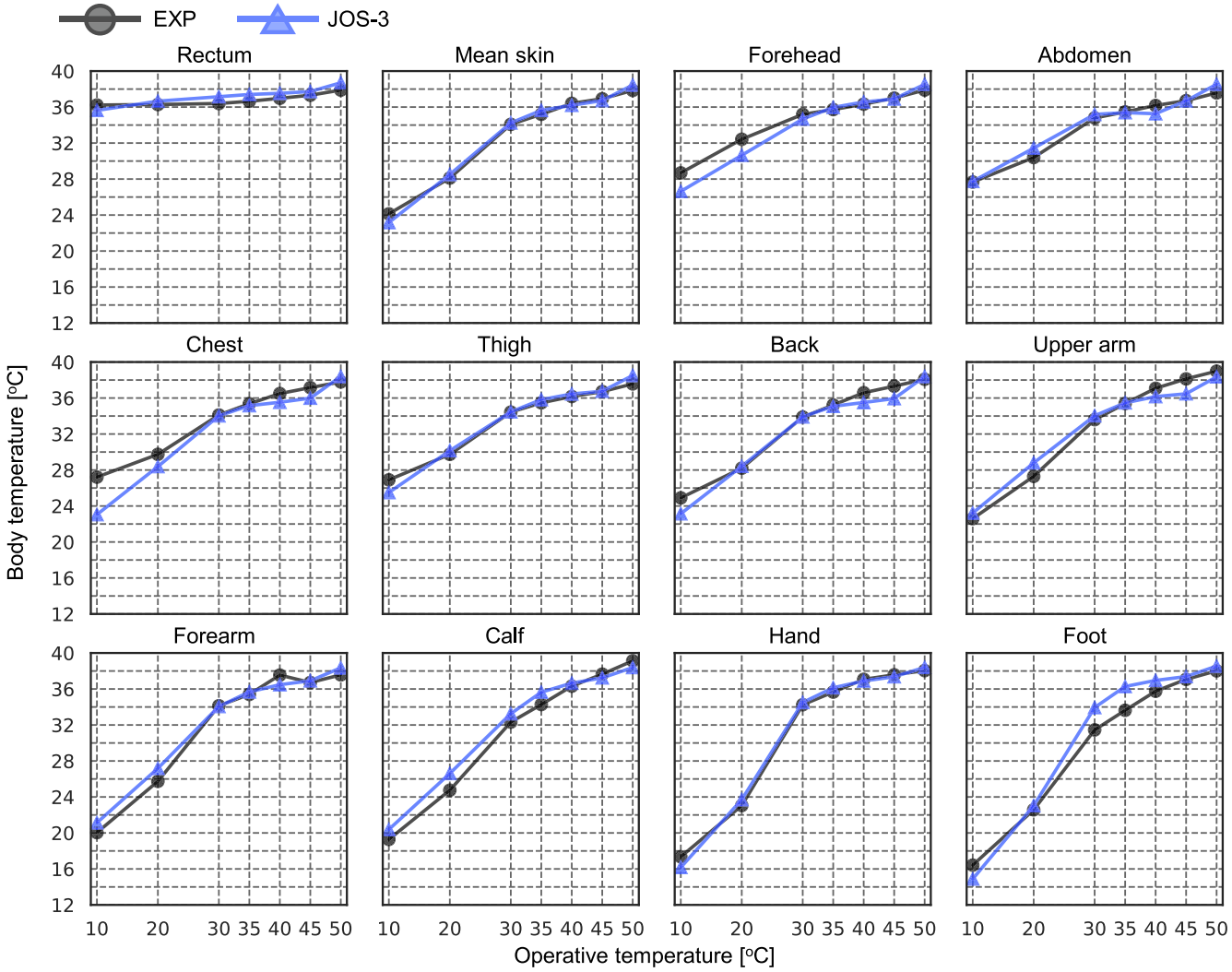

Fig. 3. Comparison between the data from Werner and Reents [48] (EXP) and predicted data (JOS-3).

Table 13
Mean error (ME), standard deviation (SD), mean absolute error (MAE), and root mean-squared error (RMSE) of body temperature [°C] between the data from Werner and Reents [48] (EXP) and predicted data (JOS-3) in six experimental conditions.

Body name	ME	SD	MAE	RMSE
Rectum	0.44	0.49	0.61	0.63
Mean skin	0.03	0.54	0.42	0.50
Forehead	−0.48	1.05	0.79	1.08
Abdomen	0.21	0.67	0.50	0.66
Chest	−1.05	1.54	1.22	1.77
Thigh	0.09	0.73	0.49	0.68
Back	−0.55	0.84	0.70	0.95
Upper arm	−0.08	1.06	0.83	0.99
Forearm	0.38	0.83	0.70	0.86
Calf	0.64	0.95	0.97	1.09
Hand	0.02	0.62	0.47	0.57
Foot	0.87	1.43	1.31	1.59

mental conditions. The predicted rectal temperatures were the pelvis core temperatures of JOS-2 and JOS-3. The MAE and RMSE of the rectal temperature were 0.13–0.37 and 0.12–0.38 °C, respectively. The prediction accuracy of Fiala's model under the temperature transients conditions was 0.10–0.25 °C RMSE for the rectal temperature [14]; therefore, RMSE of the rectal temperature prediction of JOS-3 was approximately 0.1–0.2 °C higher than that of Fiala's model. In the conditions of B-Figs. 3 and 4, which were combinations of a cold environment and hot environment, the standard deviation (SD) of the rectal temperature was higher than that in other conditions. Fig. 4 shows that the increase and decrease in the predicted rectal temperature moved in the opposite direction from the measured value. It is considered that the accuracy of predicting the rectal temperature of JOS-3 decreases in severely cold and hot environments. Except for A-Fig. 4, the MAE and RMSE for the mean skin temperature were 0.47–0.68 and 0.58–0.83 °C, respectively. The experimental mean skin temperature of A-Fig. 4 was lower than that of A-FIG.5–7 at 28 °C. The results indicated that the tendency of the measured data of A-Fig. 4 was different for the other conditions. The RMSE of the mean skin temperature under the temperature transient condition of Fiala's model was 0.30–0.78 °C [14], and approximately similar to that of JOS-3.

11. Discussion

11.1. Advantages and disadvantages

The features of JOS-3 include the control of arteriovenous anastomosis (AVA) blood flow and non-shivering thermogenesis (NST) are installed. We consider that the AVA control improves skin tem-

Table 14
Input conditions to simulate Stolwijk and Hardy's experiments [49,50].

(a) Experimental schedule

		Preparation	Phase 1	Phase 2	Phase 3
Time	[min]	60	60	120	60
Relative humidity	[%]	40	40	40	40
Air velocity	[°C]	0.1	0.1	0.1	0.1
PAR	[–]	1.2	1.2	1.2	1.2
Operative temp.	[°C]	28	Variable value		

(b) Operative temperatures [°C] in nine experiments

Literature	Conditions	Phase 1	Phase 2	Phase 3
A: Stolwijk and Hardy (1966) [49]	A-Fig.4	27.8	33.3	28.0
	A-Fig.5	28.5	37.5	28.5
	A-Fig.6	28.0	42.5	28.1
	A-Fig.7	28.1	47.8	28.3
B: Hardy and Stowijk (1966) [50]	B-Fig.1	29.0	22.0	29.0
	B-Fig.2	28.0	18.0	28.0
	B-Fig.3	22.3	43.5	22.6
	B-Fig.4	18.0	42.0	18.0
	B-Fig.5	43.0	17.0	43.0

(c) Subjects' information

Literature	Subject	Height [m]	Weight [kg]	Age [year]
A: Stolwijk and Hardy (1966) [49]	VB	1.95	88.6	25
	JA	1.84	76.1	22
	AS	1.75	110	23
B: Hardy and Stowijk (1966) [50]	RM	1.91	77.2	25
	MH	1.91	84.5	22
	HM	1.88	92.7	23

perature prediction accuracy in mildly hot environments, whereas the NST control improves the heat production prediction accuracy in mildly cold environments. Because the limb segments of JOS-3 are divided into left and right contrasting Stolwijk's model [8], it is suitable for non-uniform thermal environment evaluation. Conversely, Stolwijk's model is composed of four layers in each segment, while JOS-3 is composed of two layers, except the head and pelvis. Furthermore, heat transfer in two dimensions due to conduction is not considered, for example, the heat exchange of conduction in adjacent skin segments. This simplifies the calculation when coupling CFD and JOS-3. However, JOS-3 has four layers in the head and pelvis because the two layers did not provide sufficient prediction accuracy.

11.2. Studies to support assumptions

The basic physical properties of JOS-3 were derived from Stolwijk's model. Moreover, the controls of AVA blood flow and NST, which are not in Stolwijk's model, were also constructed based on previous studies. However, there is insufficient data related to the setpoint temperature, shivering thermogenesis, and outdoor environment. It is assumed that the setpoint temperatures of thermoregulation are defined as calculated body temperatures of JOS-3 under the thermoneutral environment based on PMV- model [1]. Furthermore, the limitation of the amount of change in shivering thermogenesis is estimated based on the experimental results [40]. Although we showed the method of the heat gain on the skin by the shortwave solar radiation, there is not sufficient human subject experiment data to validate the model. In this sense, further investigation is required.

11.3. Applicability

JOS-3 does not have ethnic restrictions, but some minor changes are required when predicting physiology for a certain group of people with high accuracy. For example, body size, age, and sex are used as variables in the equations for calculating heat production, but the proportion of body tissues is not considered. Thus, it is necessary to change the heat production equation depending on the group ethnicity since body composition differs slightly in each ethnic group. Furthermore, since hot acclimation is not considered in this model, JOS-3 may not be able to accurately predict the sweating rate of people living in hot areas such as Southeast Asia. Therefore, the parameters related to sweat rate are changed based on the actual data for a specific ethnic group when predicting the physiological responses for that group of people with high accuracy.

In simulating experiments of Werner and Reents [48] and Stowlijk and Hardy [49,50], the limit of the skin wittedness, $w_{[i]}$, was set to 1.0 because Gagge et al. reported that $w_{[i]}$ did not exceed 0.7 to 1.0 [7]. Meanwhile, when Esw/Emax is 1.0, the effective skin wettedness is calculated as approximately 0.7 from Alber–Wallerström and Holmér's regression equation [53]. In their experiment, the sweat was more likely to drip more than in the rest condition since the subject exercised on a bicycle ergometer. Therefore, it is desirable to change the upper limit of $w_{[i]}$ depending on the activity in the range of 0.7 to 1.0 [7].

11.4. Limitations and future works

To improve the accuracy of JOS-3, it is necessary to review the heat production, basal blood flow, and study the modeling method of clothing. In these simulations, the predicted results of JOS-3 were significantly affected by changes in heat production and basal blood flow when we analyzed the sensitivity of the model to these features. Additionally, because JOS-3 models clothing as thermal resistance, the heat capacity, moisture absorption, and release property of clothing are not considered. This can be a factor that deteriorates the prediction accuracy when wearing heavy clothing conditions or in the occurrence of pumping effects of clothing. Accordingly, it is necessary to study clothing modeling methods in the future.

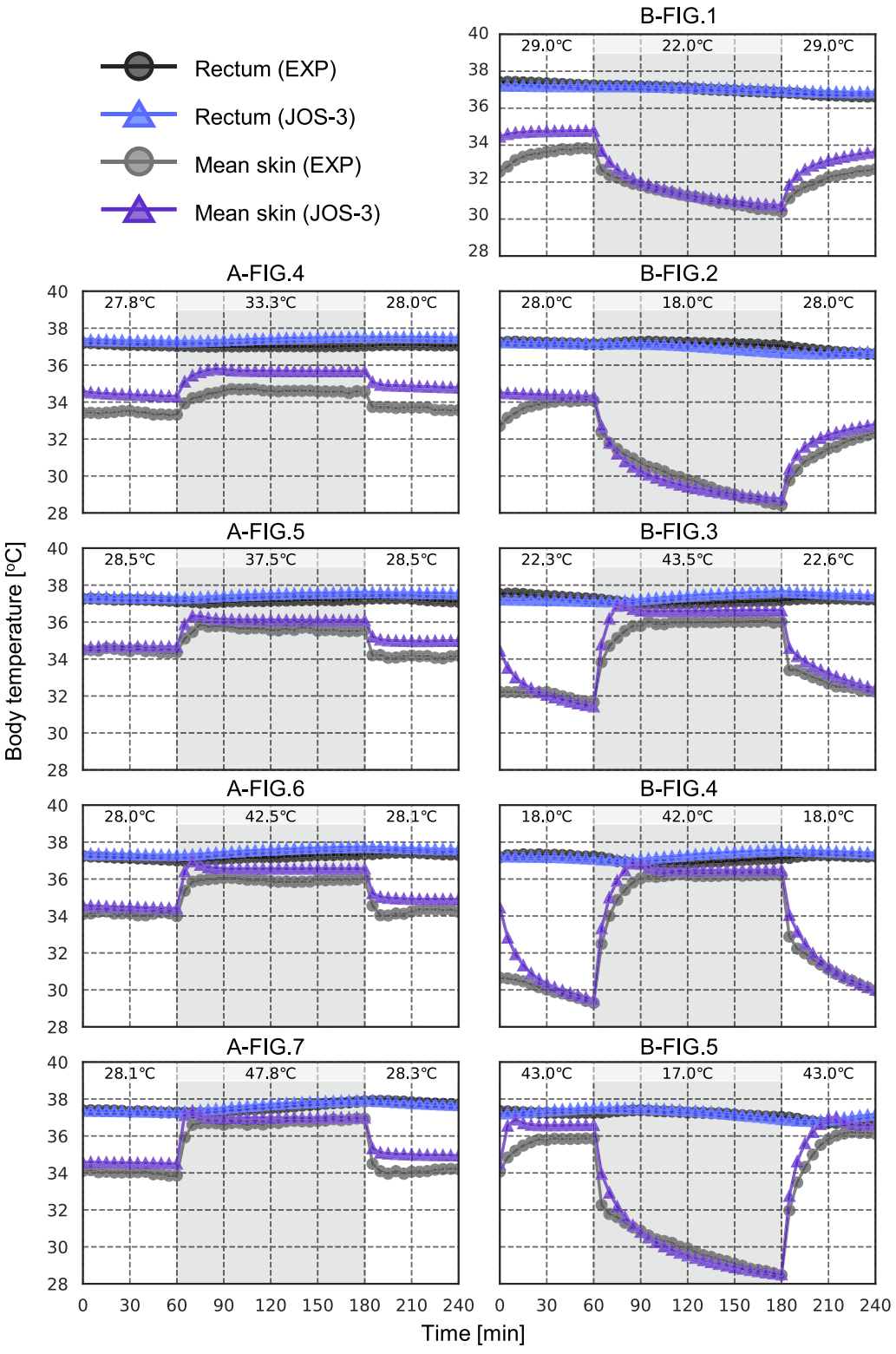

Fig. 4. Comparison between the data from Stolwijk and Hardy [49,50] (EXP) and predicted data (JOS-3).

12. Conclusion

- We developed a human thermoregulation model, JOS-3, to predict human physiological responses considering personal characteristics in transient and non-uniform thermal environments. This model was developed based on JOS-2, which was developed by our research team. The main differences between JOS-3 and JOS-2 are as follows:
- Heat gain due to short wavelength radiation was added to the heat balance equation at the skin layer to predict human body temperatures more accurately in a solar radiation environment.

Table 15
Mean error (ME), standard deviation (SD), mean absolute error (MAE), and root mean-squared error (RMSE) of body temperature [°C] between the data from Stolwijk and Hardy [49,50] (EXP) and predicted data (JOS-3).

Experiment	Body name	ME	SD	MAE	RMSE
A-Fig 4	Rectum	0.37	0.11	0.37	0.38
	Mean skin	1.11	0.11	1.11	1.11
A-fig.5	Rectum	0.30	0.11	0.30	0.32
	Mean skin	0.52	0.26	0.52	0.58
A-Fig.6	Rectum	0.31	0.09	0.31	0.33
	Mean skin	0.60	0.20	0.60	0.63
A-Fig.7	Rectum	0.07	0.10	0.09	0.12
	Mean skin	0.50	0.31	0.50	0.59
B-Fig.1	Rectum	0.04	0.13	0.11	0.13
	Mean skin	0.68	0.49	0.68	0.83
B-Fig.2	Rectum	−0.11	0.13	0.13	0.17
	Mean skin	0.27	0.51	0.47	0.58
B-Fig.3	Rectum	0.18	0.28	0.31	0.33
	Mean skin	0.59	0.50	0.64	0.77
B-Fig.4	Rectum	0.21	0.23	0.26	0.30
	Mean skin	0.52	0.64	0.52	0.82
B-Fig.5	Rectum	0.10	0.13	0.13	0.16
	Mean skin	0.46	0.61	0.60	0.76

- Metabolic rate, which is an input condition of JOS-3, can vary according to height, weight, age, and gender. In this model, the metabolic rate is calculated by multiplying the basal metabolic rate, which is estimated using the Harris–Benedict equation with PAR.
- NST control was added based on a previous study. In JOS-3, heat production changes depending on BMI and age.
- An aging factor of the cardiac index was added. The shivering heat production was proportional to the decay of the basal metabolic rate; the attenuation coefficients of vasodilation and sweating were assigned to each part of the body, based on the values in the literature.
- To compare the accuracy of JOS-2 and JOS-3, the experiments by Inoue et al. were simulated. Excessive heat production in JOS-2 decreased in JOS-3, and its prediction accuracy improved in all experimental conditions. Conversely, low heat production led to a decrease in the rectal temperature of JOS-3, and MAE and RMSE of the rectal temperature in JOS-3 increased in the three conditions. The prediction accuracy of mean skin temperature was higher in JOS-3 than in JOS-2 in the conditions of older people.
- To examine the basic performance of JOS-3 in a stable environment, the experiments by Werner and Reents were simulated. The measured rectal temperature, mean skin temperature, and 10 local skin temperatures under operative temperatures of 10, 20, 30, 35, 40, 45, and 50 °C were compared to those predicted by JOS-3. Consequently, JOS-3 tended to underestimate body temperature under 10 °C operative temperatures.
- To examine the basic performance of JOS-3 in a transient environment, the experiments of Stolwijk and Hardy were simulated. The measured and predicted values of rectal temperature and mean skin temperature under nine conditions were compared. Consequently, the MAE and RMSE of the rectal temperature were 0.13–0.37 and 0.12–0.38 °C, respectively. Those of the mean skin temperature were 0.47–0.68 and 0.58–0.83 °C, respectively. In the environment away from neutral, the prediction accuracy for the rectal temperature of JOS-3 tended to decrease.
- We showed insufficient data and improvement points for the model. Data relating to the setpoint temperatures, sieving thermogenesis, and human subject experiments in outdoor environments are required to support the assumptions of the model. In addition, it is necessary to review the heat production and basal blood flow, and the modeling of clothing may improve the accuracy of JOS-3.

Funding

This work was supported by the Japan Society for Promotion of Science (grant numbers 19H00797 and 20 J14702).

CRediT authorship contribution statement

Yoshito Takahashi: Conceptualization, Methodology, Software, Validation, Formal analysis, Investigation, Data curation, Writing - original draft, Visualization. **Akihisa Nomoto:** Investigation, Writing - review & editing, Visualization. **Shu Yoda:** Investigation, Writing - review & editing. **Ryo Hisayama:** Investigation, Writing - review & editing. **Masayuki Ogata:** Investigation, Writing - review & editing. **Yoshiichi Ozeki:** Methodology, Investigation, Writing - review & editing. **Shin-ichi Tanabe:** Methodology, Writing - review & editing, Supervision, Project administration.

Declaration of Competing Interest

The authors declare that they have no known competing financial interests or personal relationships that could have appeared to influence the work reported in this paper.

Acknowledgements

The authors would like to thank Yutaka Kobayashi, Hiroki Miyajima, and Jun-ichi Asaka (graduates of Waseda University) for their assistance with conceptualization and methodology, and Miyoko Oiwake and Yuya Hoshi (AGC corp.) for their formal analysis.

References

[1] P.O. Fanger, Thermal comfort: analysis and applications in environmental engineering, R.E. Krieger Pub. Co., Malabar Florida U.S.A., 1982.
[2] A.P. Gagge, J.A.J. Stolwjk, Y. Nishi, An effective temperature scale based on a simple model of human physiological regulatory response, ASHRAE Trans. 77 (1971) 247–263.
[3] R.J. De Dear, T. Akimoto, E.A. Arens, G. Brager, C. Candido, K.W.D. Cheong, B. Li, N. Nishihara, S.C. Sekhar, S. Tanabe, J. Toftum, H. Zhang, Y. Zhu, Progress in thermal comfort research over the last twenty years, Indoor Air 23 (6) (2013) 442–461, https://doi.org/10.1111/ina.12046.
[4] D. Filingeri, H. Zhang, E.A. Arens, Thermosensory micromapping of warm and cold sensitivity across glabrous and hairy skin of male and female hands and feet, J. Appl. Physiol. 125 (2018) 723–736, https://doi.org/10.1152/japplphysiol.00158.2018.
[5] M. Luo, Z. Wang, H. Zhang, E. Arens, D. Filingeri, L. Jin, A. Ghahramani, W. Chen, Y. He, B. Si, High-density thermal sensitivity maps of the human body, Build. Environ. 167 (2020), https://doi.org/10.1016/j.buildenv.2019.106435 106435.

[6] E.H. Wissler, A mathematical model of the human thermal system, Bull. Math. Biophys. 26 (2) (1964) 147–166, https://doi.org/10.1007/BF02476835.
[7] A.P. Gagge, A.P. Fobelets, L.G. Berglund, A standard predictive index of human response to the thermal environment, ASHRAE Trans. 92 (2B) (1986) 709–731.
[8] J.A.J. Stolwijk, A mathematical model of physiological temperature regulation in man. NASA Contractor Report CR-1855, NASA Contract. Rep., vol. CR-1855, no. August, p. 77, 1971, doi: NASA CR-1855.
[9] J.A.J. Stolwijk, J.D. Hardy, Temperature regulation in man - A theoretical study, Pflugers Arch. Gesamte Physiol. Menschen Tiere 291 (2) (1966) 129–162, https://doi.org/10.1007/BF00412787.
[10] B.W. Jones, Y. Ogawa, Transient interaction between the human and the thermal environment, ASHRAE Trans. 98 (pt 1) (1992) 189–195.
[11] I. Kohri, T. Mochida, Evaluation method of thermal comfort in a vehicle with a dispersed two-node model part 1—Development of dispersed two-node model, J. Human-Environ. Syst. 6 (1) (2002) 19–29, https://doi.org/10.1618/jhes.6.19.
[12] I. Kohri, T. Mochida, Evaluation method of thermal comfort in a vehicle with a dispersed two-node model part 2-Development of new evaluation, J. Human-Environ. Syst. 6 (2) (2003) 77–91, https://doi.org/10.1618/jhes.6.77.
[13] R.G. Gordon, R.B. Roemer, S.M. Horvath, A mathematical model of the human temperature regulatory system–transient cold exposure response, IEEE Trans. Biomed. Eng. BME-23(6) (1976) 434–444, https://doi.org/10.1109/TBME.1976.324601.
[14] D. Fiala, K.J. Lomas, M. Stohrer, Computer prediction of human thermoregulatory and temperature responses to a wide range of environmental conditions, Int. J. Biometeorol. 45 (3) (2001) 143–159, https://doi.org/10.1007/s004840100099.
[15] C. Huizenga, Z. Hui, E. Arens, A model of human physiology and comfort for assessing complex thermal environments, Build. Environ. 36 (6) (2001) 691–699, https://doi.org/10.1016/S0360-1323(00)00061-5.
[16] R. Streblow, Thermal sensation and comfort model for inhomogeneous indoor environments, E.ON Energy Research Center. RWTH Aachen Univ., 2010. url: https://d-nb.info/1018222863/34
[17] C.E. Smith, A transient, three-dimensional model of the human thermal system, Ph.D. Thesis, Kansas State Univ. (1991), https://doi.org/10.16953/deusbed.74839.
[18] T. Takemori, T. Nakajima, Y. Shoji, A fundamental model of the human thermal system for prediction of thermal comfort, Trans. Japan Soc. Mech. Eng. B. 61 (584) (1995) 1513–1520, https://doi.org/10.1299/kikaib.61.1513.
[19] G. Fu, A Transient, 3-D mathematical thermal model for the clothed human, KSU, Dissertation (1995).
[20] J. Werner, M. Buse, Temperature profiles with respect to inhomogeneity and geometry of the human body, J. Appl. Physiol. 65 (1988) 1110–1118. doi: 0.1152/jappl.1988.65.3.1110.
[21] S. Tanabe, K. Kobayashi, J. Nakano, Y. Ozeki, M. Konishi, Evaluation of thermal comfort using combined multi-node thermoregulation (65MN) and radiation models and computational fluid dynamics (CFD), Energy Build. 34 (6) (2002) 637–646, https://doi.org/10.1016/S0378-7788(02)00014-2.
[22] T. Sato, L. Xu, K. Ogawa, S. Tanabe, Development of human thermoregulation model JOS applicable to different types of human body, sex and age, in: Heal. Build. 2003 - Proc. 7th Int. Conf. (7th-11th December 2003) - Natl. Univ. Singapore, vol. 1., pp. 828–834.
[23] Y. Kobayashi, S. Tanabe, Development of JOS-2 human thermoregulation model with detailed vascular system, Build. Environ. 66 (2013) 1–10, https://doi.org/10.1016/j.buildenv.2013.04.013.
[24] J.A. Wagner, S.M. Horvath, Influences of age and gender on human thermoregulatory responses to cold exposures, J. Appl. Physiol. 58 (1985) 180–186. doi: org/10.1152/jappl.1985.58.1.180.
[25] S. Yokoyama, N. Kakuta, T. Togashi, Y. Hamada, M. Nakamura, K. Ochifuji, Development of prediction computer program of whole body temperatures expressing local characteristic of each segment: Part1 – Bio-heat equations and solving method, Soc. Heating, Air-Conditioning Sanit. Eng. Jpn. 25 (77) (2000) 1–12, https://doi.org/10.18948/shase.25.77_1.
[26] S. Yokoyama, N. Kakuta, T. Togashi, Y. Hamada, M. Nakamura, K. Ochifuji, Development of prediction computer program of whole body temperatures expressing local characteristic of each segment: Part2 - Analysis of the mathematical model for the control of skin blood flow, Soc. Heating, Air-Conditioning Sanit. Eng. Jpn. 25 (78) (2000) 1–8, https://doi.org/10.18948/shase.25.78_1.
[27] J.W. Mitchell, G.E. Myers, An analytical model of the counter-current heat exchange phenomena, Biophys. J. 8 (8) (1968) 897–911, https://doi.org/10.1016/S0006-3495(68)86527-0.
[28] M. Ichihara, M. Saito, M. Nishihara, S. Tanabe, Measurement of convective and radiative heat transfer coefficients of standing and sitting human body by using a thermal manikin, J. Archit. Plan. (Trans. AIJ) 62 (1997) 45–51, https://doi.org/10.3130/aija.62.45_5.
[29] Y. Kurazumi, J. Ishii, K. Fukagawa, Y. Yamato, K. Tobita, T. Tsuchikawa, M. Matsubara, Body heat balance for evaluation of sleep environment: Measurements of radiative and connective heat transfer coefficients of the human body with supine position by using a thermal mannequin, Jpn. Soc. Physiol. Anthropol. 13 (2008) 17–26, https://doi.org/10.20718/jjpa.13.1_17.
[30] D.T. Reindl, W.A. Beckman, J.A. Duffie, Diffuse fraction correlations, Sol. Energy 45 (1) (1990) 1–7, https://doi.org/10.1016/0038-092X(91)90123-E.
[31] S. Watanabe, T. Hirokoshi, Calculation of mean radiant temperature in outdoors based on measurements, Japan J. Biometeor. 49 (2) (2012) 49–59, https://doi.org/10.11227/seikisho.49.49.
[32] D. Du Bois, E.F. Du Bois, A formula to estimate the approximate surface area if height and weight be known. 1916., Nutrition 5(5) (1989) 303.
[33] W.D. Van Marken Lichtenbelt, J.W. Vanhommerig, N.M. Smulders, J.M.F.L. Drossaerts, G.J. Kemerink, N.D. Bouvy, P. Schrauwen, G.J. Jaap Teule, Cold-activated brown adipose tissue in healthy men, N. Engl. J. Med. 360 (15) (2009) 1500–1508, https://doi.org/10.1056/NEJMoa0808718.
[34] M. Saito et al., High incidence of metabolically active brown adipose tissue in healthy adult humans: Effects of cold exposure and adiposity, Diabetes 58 (7) (2009) 1526–1531, https://doi.org/10.2337/db09-0530.
[35] J. Asaka, H. Miyajima, M. Ogata, S. Tanabe, Development of thermoregulation model by considering cold acclimation and simulation of thermal sensation change, Proc. ICHES2016 Nagoya (2016), Nagoya, Japan.
[36] J.A. Harris, F.G. Benedict, A biometric study of human basal metabolism, Proc. Nat. Acad. Sci. USA 4 (12) (1918) 370–373, https://doi.org/10.1073/pnas.4.12.370.
[37] A.M. Roza, H.M. Shizgal, The Harris Benedict equation reevaluated: Resting energy requirements and the body cell mass, Am. J. Clin. Nutr. 40 (1984) 168–182, https://doi.org/10.1093/ajcn/40.1.168.
[38] J. Fao, U.N.U.E. Consultation, Human energy requirements: Report of a joint FAO/ WHO/UNU expert consultation, Food Nutr. Bull. 26 (1) (2005) 166.
[39] Y. Matsumura, S. Sasaki, S.X. Han, T. Ozawa, T. Yoneshiro, M. Saito, Activity and volume of human brown adipose tissue assessed by FDG-PET/CT, Jpn. Soc. Study Obes. 19 (2013) 47–51.
[40] Y. Tochihara, T. Ohnaka, S. Yamazaki, M. Tonaka, K. Yoshida, "Heart rate and body temperature responses during and after exposure to cold, J. Anthr. Soc. Nippon 90 (4) (1982) 411–420.
[41] C. Cheng, T. Matsukawa, D.I. Sessler, M. Ozaki, A. Kurz, B. Merrifield, H. Lin, P. Olofsson, "Increasing mean skin temperature linearly reduces the core-temperature thresholds for vasoconstriction and shivering in humans, Anesthesiology 82 (5) (1995) 1160–1168.
[42] D. McLean, D. Emslie-Smith, Accidental hypothermia, Blackwell Sci. Publ, Oxford, 1977.
[43] T. Yoneshiro, S. Aita, M. Matsushita, Y. Okamatsu-Ogura, T. Kameya, Y. Kawai, M. Miyagawa, M. Tsujisaki, M. Saito, Age-related decrease in cold-activated brown adipose tissue and accumulation of body fat in healthy humans, Obesity 19 (9) (2011) 1755–1760, https://doi.org/10.1038/oby.2011.125.
[44] B.L. Strehler, Origin and comparison of the effects of time and high-energy radiations on living systems, Q. Rev. Biol. 34 (1959) 117–142, https://doi.org/10.1086/402632.
[45] Y. Inoue, M. Shibasaki, Regional differences in age related decrements of the cutaneous vascular and sweating responses to passive heating, Eur. J. Appl. Physiol. Occup. Physiol. 74 (1–2) (1996) 78–84, https://doi.org/10.1007/BF00376498.
[46] Y. Kuno, Human perspiration, American lecture series, publication no. 285. A monograph in the Bannerstone Division of American Lectures in Physiology, Charles C. Thomas (1956).
[47] Y. Inoue, M. Nakao, T. Araki, H. Ueda, "Thermoregulatory responses of young and older men to cold exposure, Eur. J. Appl. Physiol. Occup. Physiol. 65 (6) (1992) 492–498, https://doi.org/10.1007/BF00602354.
[48] J. Werner, T. Reents, A contribution to the topography of temperature regulation in man, Eur. J. Appl. Physiol. Occup. Physiol. 45 (1) (1980) 87–94, https://doi.org/10.1007/BF00421205.
[49] J.A.J. Stolwijk, J.D. Hardy, Partitional calorimetric studies of responses of man to thermal transients, J. Appl. Physiol. 21 (3) (1966) 967–977, https://doi.org/10.1152/jappl.1966.21.6.1799.
[50] J.D. Hardy, J.A.J. Stolwjk, Partitional exposures calorimetric studies of man during exposures to thermal transients, J. Appl. Physiol. 21 (1966) 1799–1806, https://doi.org/10.1152/jappl.1966.21.6.1799.
[51] A. Nomoto, Y. Takahashi, S. Yoda, M. Ogata, S. Tanabe, S. Ito, Y. Aono, Y. Yamamoto, K. Mizutani, Measurement of local evaporative resistance of typical clothing ensemble using a sweating thermal manikin, J. Environ. Eng. 84 (761) (2019) 653–660, https://doi.org/10.3130/aije.84.653.
[52] E.A. McCullough, B.W. Olesen, S. Hong, Thermal insulation provided by chairs, Symposium, ASHRAE Trans. 100 (1) (1994) 795–802.
[53] B. Alber-Wallerström, I. Holmér, Efficiency of sweat evaporation in unacclimatized man working in a hot humid environment, Eur. J. Appl. Physiol. Occup. Physiol. 54 (1985) 480–487, https://doi.org/10.1007/BF00422956.